Journal of Biomechanics 95 (2019) 109287

Contents lists available at ScienceDirect

Journal of Biomechanics

journal homepage: www.elsevier.com/locate/jbiomech
www.JBiomech.com

Skeletal kinematics of the midtarsal joint during walking: Midtarsal joint locking revisited ☆

Cong-Bo Phan [a], Geonhui Shin [b], Kyoung Min Lee [c], Seungbum Koo [a,*]

[a] Department of Mechanical Engineering, Korea Advanced Institute of Science and Technology, Daejeon, Republic of Korea
[b] School of Mechanical Engineering, Chung-Ang University, Seoul, Republic of Korea
[c] Department of Orthopedic Surgery, Seoul National University Bundang Hospital, Seongnam, Republic of Korea

ARTICLE INFO

Article history:
Accepted 29 July 2019

Keywords:
Foot
Midtarsal joint
Kinematics
Contact surface
Locking mechanism

ABSTRACT

The kinematics of the human foot complex have been investigated to understand the weight bearing mechanism of the foot. This study aims to investigate midtarsal joint locking during walking by noninvasively measuring the movements of foot bones using a high-speed bi-planar fluoroscopic system. Eighteen healthy subjects volunteered for the study; the subjects underwent computed tomography imaging and bi-planar radiographs of the foot in order to measure the three-dimensional (3D) midtarsal joint kinematics using a 2D-to-3D registration method and anatomical coordinate system in each bone. The relative movements on bone surfaces were also calculated in the talonavicular and calcaneocuboid joints and quantified as surface relative velocity vectors on articular surfaces to understand the kinematic interactions in the midtarsal joint. The midtarsal joint performed a coupled motion in the early stance to pronate the foot to extreme pose in the range of motion during walking and maintained this pose during the mid-stance. In the terminal stance, the talonavicular joint performed plantar-flexion, inversion, and internal rotation while the calcaneocuboid joint performed mainly inversion. The midtarsal joint moved towards an extreme supinated pose, rather than a minimum motion in the terminal stance. The study provides a new perspective to understand the kinematics and kinetics of the movement of foot bones and so-called midtarsal joint locking, during walking. The midtarsal joint continuously moved towards extreme poses together with the activation of muscle forces, which would support the foot for more effective force transfer during push-off in the terminal stance.

1. Introduction

The foot performs versatile functions during locomotion, and it has been suggested that the midtarsal joint, with the talonavicular and calcaneocuboid joints, contributes to the rigidity and flexibility of the foot during dynamic motions (Blackwood et al., 2005; Tweed et al., 2008). The foot was previously described to provide shock absorption in the early stance, weight support in the mid-stance, and a rigid lever arm for propulsion in the terminal stance (Tweed et al., 2008). The mechanism of transition of the foot between flexible and rigid structures during movement is thought of as a locking and unlocking mechanism (Elftman, 1960; Okita et al., 2014).

The idea of a locking and unlocking mechanism in the foot has been previously explained using the convex curvature axes of the talonavicular and calcaneocuboid articular surfaces (Elftman, 1960). Inversion or eversion of the subtalar joint changes the direction of the convex curvature axes of the talonavicular and calcaneocuboid articular surfaces, which might lock or unlock the midtarsal joint and contribute to either a rigid or flexible foot structure (Tweed et al., 2008; Elftman, 1960). For example, the subtalar joint everts at heel-strike and the convex curvature axes of the talonavicular and calcaneocuboid articular surfaces become parallel, which may increase the flexibility of the midtarsal joint. However, there is a lack of experimental evidence to suggest that the change in the axes would make the foot either flexible or rigid during walking.

Several experimental studies using cadaveric specimens have been conducted to improve the understanding of the midtarsal joint locking mechanism (Blackwood et al., 2005; Okita et al.,

☆ Each author has been involved in the design of the study, interpretation of the data, and writing of the manuscript. Each of the authors has read and concurs with the content of the manuscript.

* Corresponding author at: Department of Mechanical Engineering, Korea Advanced Institute of Science and Technology, 291 Daehak-ro, Yuseong-gu, Daejeon 34141, Republic of Korea.
E-mail address: skoo@kaist.ac.kr (S. Koo).

https://doi.org/10.1016/j.jbiomech.2019.07.031
0021-9290/

2014). It has been shown in a cadaveric foot experiment that the first, second, and fifth metatarsal bones had a significantly reduced range of rotation in the sagittal plane with respect to the coordinated system fixed in the talus when the calcaneus was inverted compared to everted (Blackwood et al., 2005). Meanwhile, the midtarsal joint remained compliant and rotations were present when the calcaneus was inverted during push-off, despite the axes of the talonavicular and calcaneocuboid joints being diverged when gait was simulated in a cadaveric foot (Okita et al., 2014). The mechanism and existence of locking in the foot during push-off has not been well investigated.

The movements of individual bones in the midfoot during *in vivo* walking has been investigated using reflective markers and metallic pins inserted in individual bones (Nester et al., 2002, Nester et al., 2007, Leardini et al., 2007). Although most of the joints in the midfoot had continuous movements during late stance, they could not insert bone pins in the talus, and they did not measure the motion in the talonavicular joint. Thus, it may have had continuous movement along with its adjacent joints, which made us revisit the definition and existence of midtarsal joint locking especially in the talonavicular and calcaneocuboid joints of intact feet during walking. Recent advances in radiographic imaging techniques has enabled dynamic measurements of *in vivo* skeletal motions in the foot, including the talus (Koo et al., 2015, Phan et al., 2018, Wang et al., 2016).

This study aims to investigate the relative motion in the talonavicular and calcaneocuboid joints that comprise the midtarsal joint during the stance phase of walking of intact feet, especially in the early and terminal stance phases that are responsible for the locking and unlocking mechanism in the foot. We used a bi-planar fluoroscopic imaging system and calculated the skeletal motion directly from the images for visualization and quantification of the relative motions on articular surfaces. The relative motions on articular surfaces and conventional rotations around joint axes were quantified during walking to understand the contribution of individual joint motions on the locking mechanism at the terminal stance. We hypothesized that the relative motions on articular surfaces in the talonavicular and calcaneocuboid joints would be minimal at the terminal stance of walking in intact feet because of joint locking in the midtarsal joint.

2. Method

2.1. Data acquisition

The study was approved by the Institutional Review Board of Chung-Ang University. Eighteen healthy males, with no history of pain and abnormal deformities in the foot and ankle, participated in this study. Informed consent was obtained from each subject prior to testing. The average (±SD) age, height, and weight of all subjects were 23.2 ± 1.8 years, 173.2 ± 5.7 cm, and 70.9 ± 6.4 kg, respectively. Each subject underwent computed tomography (CT) using the Optima CT660 CT scanner (GE Healthcare, Chicago, USA). The in-plane image had 512 × 512 pixels, and each pixel was equivalent to 0.59 mm × 0.59 mm. The number of CT slices (images) changed depending on the foot size, and the slice thickness was 0.67 mm. Polygonal models of the talus, navicular, calcaneus, and cuboid bones were then segmented and reconstructed using Seg3D software (CIBC, Salt Lake City, UT, USA). The subjects were instructed to walk along an elevated walkway made of high-strength polystyrene foam. They practiced this for 5 to 10 min until they could walk naturally. Bi-planar fluoroscopic images were taken for the right foot during a walking trial at the speed of 100 frames per second with a 0.1 ms exposure time, 1024 × 1024-pixel resolution, and 14-bit depth image. The average stance time was 683 ± 52 ms. The three-dimensional (3D) models of the talus, navicular, calcaneus, and cuboid were registered to the bi-planar fluoroscopic images using custom 2D-to-3D registration software (Koo et al., 2015). The orientations and positions of the bones were determined for the stance period of walking, which was 683 ± 52 ms, or around 70 frames, as shown in Fig. 1. The accuracy of the 2D-to-3D registration method used to measure the ankle joint *in vivo* was reported to be approximately 0.63° in orientation and 0.3 mm in translation (Wang et al., 2015).

2.2. Three-dimensional kinematics in the midtarsal joint

Bi-planar fluoroscopic images of the foot at standing posture were obtained in order to determine the standard bone positions. The anatomical coordinate systems (ACS) of the talus and calcaneus were defined based on the talar-dome and posterior talar articular surfaces at standing position using the automatic bone template registration algorithm (Phan and Koo, 2015) described in our previous study. The ACS origins of the navicular and cuboid were set at the center of the talar head and the center of the cuboid model, respectively. The ACS orientations of the navicular and cuboid were set the same as the talus and calcaneus. Thus, the ACS of all bones had the same orientation at the standing position, as shown in Fig. 1.

Rotational motions in the talonavicular and calcaneocuboid joints were quantified using the ACS, according to the joint coordinate system used in a previous study (Grood and Suntay, 1983; Wu et al., 2002). The dorsiflexion/plantar-flexion, inversion/eversion, and internal/external rotation angles in the two joints were calculated from the heel-strike to toe-off during normal walking. The frames of the stance period were determined from the bi-planar fluoroscopic images, and the frame time was normalized as 0% to 100% of the stance phase. The temporal rotational kinematics were averaged for all subjects for the stance phase, and the rotational ranges of motion (ROMs) of the two joints were quantified for the stance phase of walking.

2.3. Surface motion in the midtarsal joint

The relative surface motions in the joints were visualized and quantified. The boundaries of the articular surfaces of midtarsal

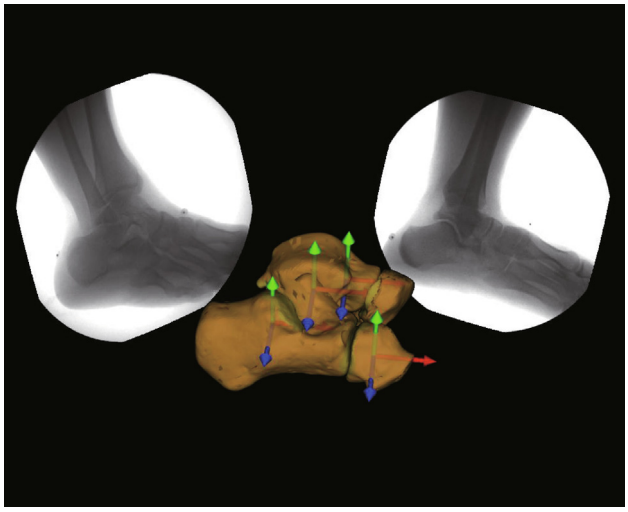

Fig. 1. Three-dimensional poses of the talus, calcaneus, navicular, and cuboid were determined using bi-planar fluoroscopic images. The anatomical joint coordinate systems of the bones were identified using the bi-planar images obtained at standing position.

joint (Fig. 2A) were determined in the bone models using our automatic bone template registration algorithm (Phan and Koo, 2015). The distances between the closest vertex pairs in the articular surfaces were calculated for all vertices inside the boundaries, and visualized as color maps for each frame as shown in Fig. 2.

The transformation matrices, or motions, of the bones were interpolated so that we could resample the bone poses at every 1% of the stance phase. We chose bone poses at every 10% between 0% and 90% of the stance phase, i.e., ten time points, to quantify the relative surface motion. We resampled up to 90% because the bone pose at toe-off, or 100% of the stance phase, was not available for most trials. Surface relative velocity vectors (SRVVs) were calculated for all vertices inside the boundaries (1911 vertices for talus and 1688 vertices for calcaneus) using the movements of the closest vertex pairs between the 10% time interval, and visualized as arrows at the vertices, as shown in Fig. 2B (Anderst and Tashman, 2010; Phan et al., 2018).

Once the SRVVs were calculated for the two joints in all 18 subjects, they were averaged vertex-wise because the sampled vertices were at similar anatomical locations between subjects. The SRVVs on the articular surface of each joint were averaged in order to calculate the average direction of the motion on the surface; this is represented as green solid lines in Fig. 2C. The average direction of motion was used to understand the main motion and kinematic interaction in the midtarsal joint. In the polar density map, the distribution of directions and magnitudes of projected SRVVs could visually represent kinematics on the articular contact surface (Fig. 2D), which helps in understanding the relative dominance of translation and rotation on the surface.

A plane was determined that best fit the 1911 vertices on the talus, and the SRVVs at the vertices were projected onto the plane. We generated a polar density map of the velocity vectors using their polar directions and lengths (Rodríguez et al., 2014; Botev et al., 2010). The process was repeated for the SRVVs on the calcaneus. The polar density map was used to qualitatively classify the contact motion into either translation or rotation on the surfaces of midtarsal joint during walking (Phan et al., 2018).

3. Results

The period of motion measured by the bi-planar fluoroscopic system was from 0% to at least 93% (Koo et al., 2015) of the stance phase for 18 subjects. In some subjects, the ankle moved outside of the imaging field of view before the toe-off. The kinematic patterns of the two joints comprising the midtarsal joint were qualitatively different at the terminal stance of walking, as shown in Fig. 3. In the early stance phase, both the talonavicular and calcaneocuboid joints showed dorsiflexion, eversion, and external rotation from heel-strike to approximately 10% of the stance phase. During the mid-stance phase (up to 72% of the stance phase), both joints had relatively smaller rotational motions in all three directions than during the early and terminal stance phases. The rotational kinematics of the talonavicular and calcaneocuboid joints had similar ROMs in dorsiflexion/plantar-flexion (11.2° vs. 12.9°) and inversion/eversion (14.5° vs. 15.8°), but the talonavicular joint had a significantly larger ROM than the calcaneocuboid joint in internal/external rotation (14.9° vs. 11.5°), as summarized in Table 1. However, in the terminal stance phase, between 72% and 93% of the stance phase, the talonavicular joint had plantarflexion, inversion, and internal rotation, while the calcaneocuboid joint had mainly inversion rotation.

The average SRVVs on the talonavicular and calcaneocuboid joints were calculated for every 10% of the stance phase, as shown in Fig. 4A. In the talonavicular joint, the average magnitudes of the velocity vectors were 31 mm/s and 46 mm/s for the early and terminal stance phases, respectively (Table 2). In the early stance, the talonavicular joint was externally rotated and everted, but in the terminal stance the talonavicular joint had a motion in the opposite direction, according to the distribution of the velocity vectors. In the calcaneocuboid joint, the SRVVs on the articular surface of the calcaneus generally headed in a medial-superior direction (Fig. 4A), and showed an inversion rotation pattern (Fig. 3) in the terminal stance. During the mid-stance, the magnitudes of the velocity vectors in the calcaneocuboid joint were less than 17 mm/s from 10% to 80% of the stance phase.

The polar density maps of the SRVVs (Fig. 4B and C) demonstrate the distribution of modules (length of SRVV in a polar coordinate system) and the directions of velocity vectors on articular surfaces. The average modules, range of direction, and maximum density of the SRVVs on the articular surfaces of the talonavicular and calcaneocuboid joints are outlined in Table 3. The density map revealed that the SRVVs in the talonavicular and calcaneocuboid joints had larger modules in the early and terminal stances than in the mid-stance. The SRVVs in both joints had opposite directions between the early and terminal stances. During the mid-stance, the SRVVs in the talonavicular joint were fairly homogeneous with red regions (density > 0.03) in the polar density map.

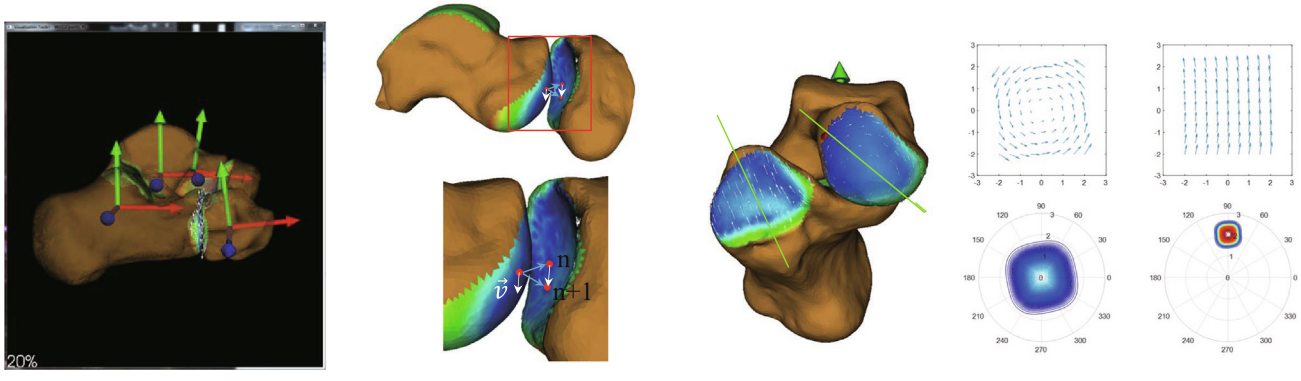

Fig. 2. (A) Anatomical coordinate system and articular surfaces on the midtarsal joint; (B) surface relative velocity vectors (SRVVs; $\vec{v}$) were calculated for each vertex on the articular surface, based on the movements of the closest vertex pairs between the 10% time interval during the stance phase; (C) SRVVs (white arrows) and average motion directions (green solid line) on the articular surfaces at a time point; (D) The SRVVs on each contact surface were projected to a plane fitted to the contact surface, and the distribution of their directions and magnitudes were plotted using a polar density to quantify to better visualize a rotational pattern (left) and a translational pattern (right). (For interpretation of the references to color in this figure legend, the reader is referred to the web version of this article.)

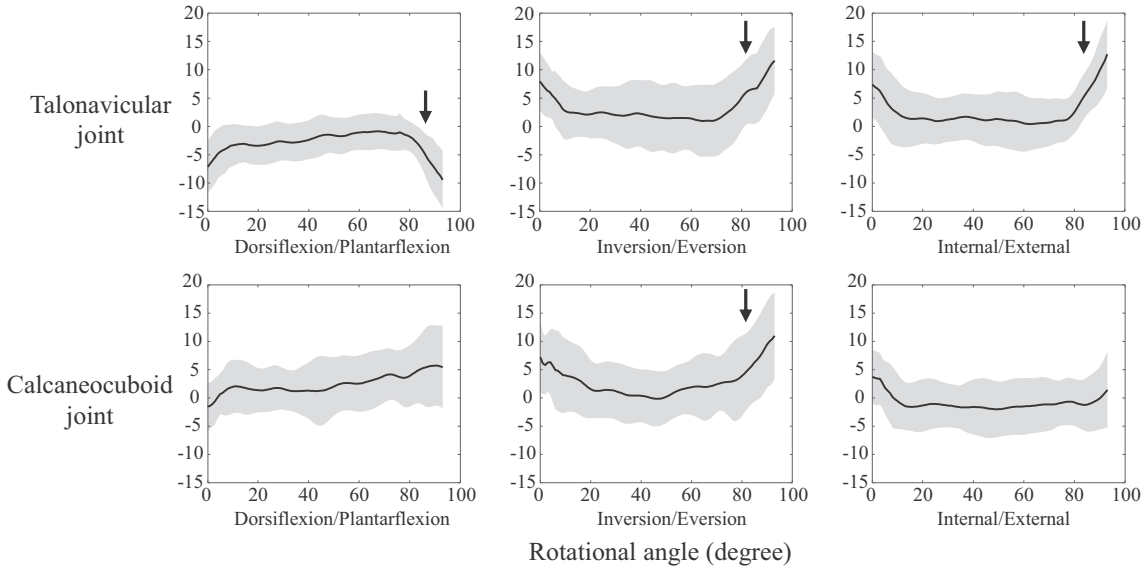

Fig. 3. Average (solid line) and one standard deviation of rotational angles in the talonavicular and calcaneocuboid joints during normal walking. In the terminal stance phase, the talonavicular joint had plantar-flexion, inversion, and internal rotation, while the calcaneocuboid joint had mainly inversion rotation as marked by arrows.

Table 1
Range of motion of rotational angle in the talonavicular and calcaneocuboid joints during stance phase of normal walking.

	Dorsiflexion/plantarflexion (°)			Inversion/eversion (°)			Internal/external rotation (°)		
	Min. dorsiflexion	Max. plantarflexion	ROM	Min. Inversion	Max. Eversion	ROM	Min. internal rotation	Max. external rotation	ROM
Talo-navicular joint	0.7 ± 3.1*	10.4 ± 4.7*	11.2 ± 3.3	12.4 ± 5.5	2.1 ± 5.4	14.5 ± 4.5	13.2 ± 5.6*	1.7 ± 3.7*	14.9 ± 5.1*
Calcaneocuboid joint	9.4 ± 6.2*	3.5 ± 4.2*	12.9 ± 6.2	12.9 ± 6.3	2.9 ± 4.8	15.8 ± 4.3	5.8 ± 5.0*	5.7 ± 3.3*	11.5 ± 3.3*

* Significant at $p < 0.05$ using paired-sample t-test.

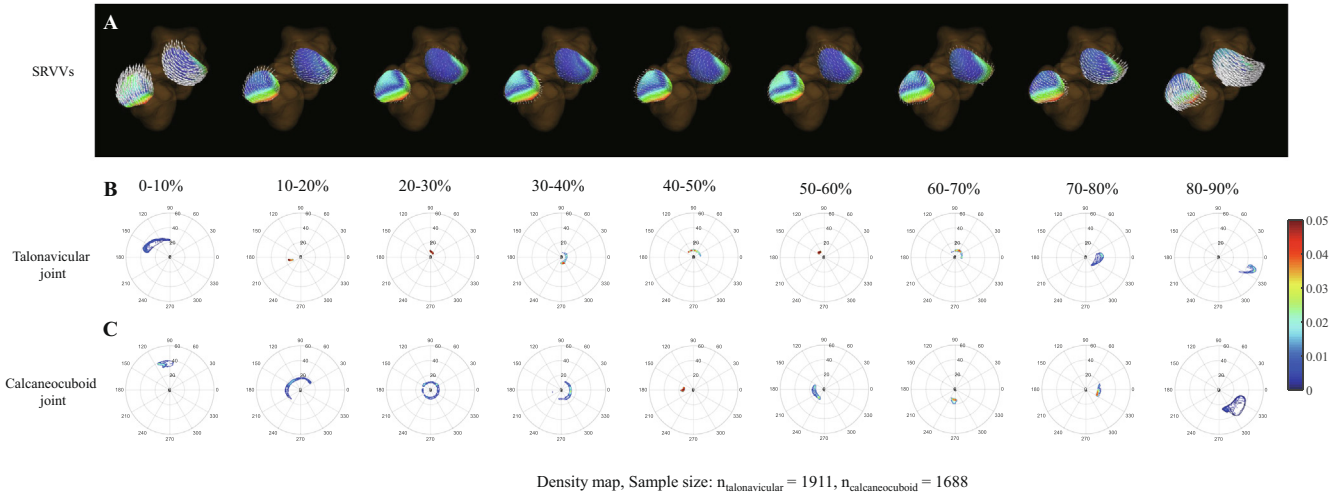

Fig. 4. Surface motion on the articular surfaces of the midtarsal joint for each 10% of stance phase: (A) surface relative velocity vectors on talonavicular and calcaneocuboid joints; (B) density map of talonavicular joint; (C) density map of calcaneocuboid joint.

The average motion directions of the talonavicular and calcaneocuboid joints were calculated and visualized as green lines on top of the SRVVs in Fig. 5, which shows the major motion in the joints. The navicular and cuboid moved superiorly and laterally in the early stance (0%–10% of the stance phase) and inferiorly and medially in the terminal stance (80%–90% of the stance phase), as shown in the density map (Fig. 4) and by the SRVVs on articular surfaces (Fig. 5). The direction of the SRVVs in the talonavicular (320°–338°) and calcaneocuboid (286°–343°) joints in the plane close to the frontal plane were fairly similar, with both heading in inferior and medial directions at the terminal stance (Table 3).

Table 2
Average (standard deviation) magnitudes of the surface relative velocity vectors (SRVVs) on articular surface of talonavicular and calcaneocuboid joints at 10% intervals of the stance phase.

	Average (std) magnitudes of the surface relative velocity vectors SRVVs (mm)								
	0–10%	10–20%	20–30%	30–40%	40–50%	50–60%	60–70%	70–80%	80–90%
Talonavicular joints	31.1 (3.9)	14.4 (1.9)	7.1 (1.0)	7.5 (0.9)	9.2 (0.4)	9.3 (0.5)	9.7 (0.8)	18.1 (3.1)	46.0 (4.6)
Calcaneocuboid joints	36.0 (2.1)	16.8 (1.3)	10.8 (0.6)	12.5 (0.6)	14.1 (1.1)	13.6 (1.1)	15.3 (1.6)	17 (1.1)	31.6 (4.7)

Table 3
Average (standard deviation) module, range of direction, and maximum density of the density map in talonavicular and calcaneocuboid joints at 10% intervals of the stance phase of walking.

	Stance phase								
	0–10%	10–20%	20–30%	30–40%	40–50%	50–60%	60–70%	70–80%	80–90%
Talonavicular joint									
Average (std) module (mm)	26.2 (14.3)	13.4 (10.0)	26.2 (14.3)	13.4 (10.0)	26.2 (14.3)	13.4 (10.0)	26.2 (14.3)	13.4 (10.0)	26.2 (14.3)
Range of direction (°)	91–160	179–201	60–98	261–68	18–139	118–139	0–126	306–9	320–338
Maximum density	0.01	0.17	0.17	0.08	0.09	0.16	0.08	0.03	0.03
Calcaneocuboid joint									
Average (std) module (mm)	27.2 (16.8)	13.9 (8.1)	9.6 (4.6)	10.5 (7.6)	10.9 (6.2)	11.3 (5.2)	12.4 (8.8)	13.1 (6.2)	24.0 (10.7)
Range of direction (°)	84–113	38–218	12–353	3–356	165–186	160–243	249–275	331–18	286–343
Maximum density	0.03	0.02	0.03	0.03	0.11	0.03	0.08	0.06	0.01

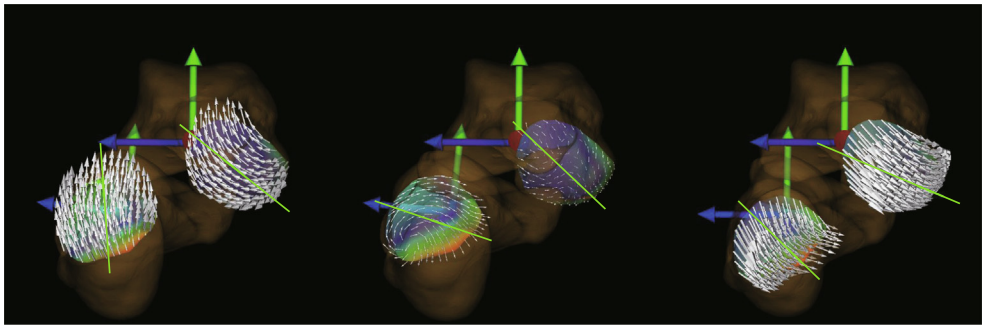

Fig. 5. Surface relative velocity vectors and average motion directions of the talonavicular and calcaneocuboid joints at 0%–10%, 30%–40%, and 80%–90% of the stance phase.

4. Discussion

The relative motions on articular surfaces in the talonavicular and calcaneocuboid joints were not minimum at the terminal stance of walking contrary to our hypothesis. The motion in the midtarsal joint was larger during the early and terminal stances than during the mid-stance of walking. The relative surface motions in the talonavicular and calcaneocuboid joints at push-off started to increase from 72% of the stance phase and continued to the terminal stance, with an opposite direction to those at the heel-strike and early stance phases. The midtarsal joint had a continuous joint motion towards extreme poses in the range of motion at the terminal stance in both the talonavicular and calcaneocuboid joints, possibly through activation of the plantar flexors of the foot and ankle.

We used both ACS and SRVV to quantify the midtarsal foot kinematics during the stance phase of walking. The joint kinematics using the ACS showed that the talonavicular and calcaneocuboid joints had rotations in the same direction during early stance. At the terminal stance, the talonavicular joint had plantarflexion, inversion, and internal rotation, while the calcaneocuboid joint had mainly inversion. The talonavicular and calcaneocuboid joints performed dorsiflexion, eversion, and external rotation during the early stance (0%–10% of the stance phase), as shown in Fig. 3, consistent with a previous report from Okita et al. (2014). The coupled motion in the early stance demonstrated that the two joints had the same rotational axis, which transformed the midtarsal joint into a more flexible position (Blackwood et al., 2005; Mann, 1975; Elftman, 1960; Manter, 1941). After the large rotational motion in the early stance, the midtarsal joint was in an extreme pronation pose, possibly because of muscle and ligament constraints during the mid-stance (Anderson and Pandy, 2003; Maharaj et al., 2016). The talonavicular and calcaneocuboid joints had different rotational movements in the terminal stance (72%–93% of the stance phase): The talonavicular joint performed plantarflexion (4.4°), inversion (10.6°), and internal rotation (20.8°) in the terminal stance (Fig. 3), while the calcaneocuboid joint performed mainly inversion (8.1°), which is consistent with previous studies using bone pins inserted in foot bones (Lundgren et al., 2008; Okita et al., 2014). This movement demonstrated that the two joints might have different rotational axes during push-off. During the stance phase, the talonavicular joint had a significantly larger ROM (Table 1) than the calcaneocuboid joint, only for the internal/external rotation (14.9° vs. 11.5°), which is likely to be caused by the convex shape of the talar head, in that its ball and socket joint allows for larger movement (Lundgren et al., 2008; Nester et al., 2001).

Complementing the ACS-based 3D rotational kinematics, the suggested SRVV provided intuitive visualization of the relative movements on the contact surfaces in the midtarsal joint during

walking to better understand the essence of midtarsal joint locking. The SRVVs on the talonavicular and calcaneocuboid joints revealed that the two joints were mainly translated and rotated during 0%–10% (31 mm/s and 36 mm/s in the talonavicular and calcaneocuboid joints, respectively) and 80%–90% (46 mm/s and 32 mm/s in the talonavicular and calcaneocuboid joints, respectively) of the stance phase, as shown in Fig. 4A, which moved the foot into an extremely pronated position at the heel strike, and an extremely supinated position at the toe-off in the range of motion during walking. In the early stance, the SRVVs on the talus and calcaneus articular surfaces were distributed around 135° and 110°, respectively (Fig. 4B), which revealed that both the talonavicular and calcaneocuboid joints had dorsi-flexion and eversion. The midtarsal joint had a small amount of motion during the mid-stance, with SRVVs of less than 20 mm/s (Fig. 4B and C). During the terminal stance, the talonavicular and calcaneocuboid joints had inversion and medial and inferior translation with the SRVVs distributed around 330° and 290°, respectively, in the plane fitted to the contact surfaces. Combining the observations in the ACS-based 3D kinematics and the SRVV-based plane kinematics, the talonavicular joint had plantar-flexion, inversion, and internal rotation raising the medial longitudinal arch of the foot, while the calcaneocuboid joint had inversion and medial and inferior translation. These extreme supinations at the midtarsal joint are likely due to a large force from the tibialis posterior muscle, which can also provide the propulsion force in the terminal stance (Hunt et al., 2001; Niki et al., 2001).

Together with movement toward extreme poses, active and passive tissues, such as muscles and ligaments, would help the foot absorb and transfer forces during the stance phase of walking. In the early stance, the tibialis posterior tendon provides tension for the subtalar joint pronation (Maharaj et al., 2017). The peroneus longus plays a role as a co-contractor with the tibialis anterior to stabilize the whole foot during the early stance (Gray and Basmajian, 1968; Hunt et al., 2001). The peroneus longus then works as a stabilizer for the foot during mid-stance (Gray and Basmajian, 1968). The push-off period started from approximately 62% of the stance phase (Hunt et al., 2001), when the anterior-posterior ground friction force pushes the body forward. The plantar flexors including tibialis posterior muscle in the foot fire at around 60% of the stance phase (Okita et al., 2014; Hunt et al., 2001) to generate forces and rotate joints. It has been reported that the tibialis posterior muscle actively shortens during the early stance and then efficiently returns the elastic strain in the terminal stance for propulsion (Maharaj et al., 2016). However, the tibialis posterior muscle is not strong enough to produce the foot propulsion force and maintain a medial longitudinal arch (Jones, 1941), but instead contributes to deformation of the foot structure (Kitaoka et al., 1997). In the terminal stance, the tibialis posterior and plantar flexor muscles activate to invert the subtalar joint, which transforms the talonavicular and calcaneocuboid movement to the extreme supinated position (Maharaj et al., 2016). The rotation of the subtalar joint, combined with the activation of the plantar flexors at the terminal stance, would support the foot for the effective transfer of force during push-off (Anderson & Pandy, 2003).

This study has several limitations. Our bi-planar fluoroscopic system has 14-inch circular image intensifiers and is not a mobile system, as shown in Fig. 1. As a result, the ankle moved outside of the field of view at the terminal stance and the joint kinematics could not be quantified. Although we have implemented several automatic 2D-to-3D registration methods, the foot radiographs were fairly challenging for our automatic registration software. Therefore, the bones were manually matched to the bi-planar fluoroscopic images. The intraclass correlation coefficient (ICC) of the registration of the tibia, talus, and calcaneus by three independent observers was 0.94 ± 0.05 in translation and 0.99 ± 0.01 in rotation, respectively. Since the foot kinetics were neither measured nor calculated in this study, we used the muscle activities and passive tissue forces that were investigated in previous studies.

In conclusion, our results are contrary to the hypothesis that the midtarsal joint had minimum relative motion at the terminal stance. The midtarsal joint had a continuous joint motion toward extreme pose, together with constraint of muscles and ligaments during the terminal stance, which would enable effective push-off. The talonavicular and calcaneocuboid joints performed a coupled motion that quickly rotated the foot to extreme pronation during the early stance and maintained the pose during the mid-stance. Then, the motion directions of the talonavicular and calcaneocuboid joints twisted against each other, while the two joints moved to the extreme supination in the terminal stance. These findings provide an additional perspective to understand the foot kinematics of so-called midtarsal joint locking and unlocking during walking.

Acknowledgement

This work was financially supported by the Basic Science Research Program through the National Research Foundation of Korea (NRF-2017R1A2B2010763) funded by the Ministry of Science and ICT of the Republic of Korea. This research was also supported by the Graduate Research Scholarship in 2018 of the Chung-Ang University, Republic of Korea.

Declaration of Competing Interests

The authors have no conflict of interest in this study. The paper has been not submitted elsewhere for publication.

Appendix A. Supplementary material

Supplementary data to this article can be found online at https://doi.org/10.1016/j.jbiomech.2019.07.031.

References

Anderson, F.C., Pandy, M.G., 2003. Individual muscle contributions to support in normal walking. Gait Post. 17 (2), 159–169.
Anderst, W.J., Tashman, S., 2010. Using relative velocity vectors to reveal axial rotation about the medial and lateral compartment of the knee. J. Biomech. 43, 994–997.
Blackwood, C.B., Yuen, T.J., Sangeorzan, B.J., Ledoux, W.R., 2005. The midtarsal joint locking mechanism. Foot Ankle Int. 26 (12), 1074–1080.
Botev, Z.I., Grotowski, J.F., Kroese, D.P., 2010. Kernel density estimation via diffusion. Ann. Stat. 38 (5), 2916–2957.
Elftman, H., 1960. The transverse tarsal joint and its control. Clin. Orthop. 16, 41–46.
Gray, E.G., Basmajian, J.V., 1968. Electromyography and cinematography of leg and foot (“normal” and flat) during walking. Anat. Rec. 161 (1), 1–5.
Grood, E.S., Suntay, W.J., 1983. A joint coordinate system for the clinical description of three-dimensional motions: application to the knee. J. Biomech. Eng. 105 (2), 36–44.
Hunt, A.E., Smith, R.M., Torode, M., 2001. Extrinsic muscle activity, foot motion and ankle joint moments during the stance phase of walking. Foot Ankle Int. 22 (1), 31–41.
Kitaoka, H.B., Luo, Z.P., An, K.-N., 1997. Effect of the posterior tibial tendon on the arch of the foot during simulated weight bearing: biomechanical analysis. Foot Ankle Int. 18, 43–46.
Koo, S., Lee, K.M., Cha, Y.J., 2015. Plantar-flexion of the ankle joint complex in terminal stance is initiated by subtalar plantar-flexion: a bi-planar fluoroscopy study. Gait Post. 42, 424–429.
Leardini, A., Benedetti, M.G., Berti, L., Bettinelli, D., Nativo, R., Giannini, S., 2007. Rear-foot, mid-foot and fore-foot motion during the stance phase of gait. Gait Post. 25 (3), 453–462.
Lundgren, P., Nester, C., Liu, A., Arndt, A., Jones, R., Stacoff, A., Wolf, P., Lundberg, A., 2008. Invasive in vivo measurement of rear-, mid-and forefoot motion during walking. Gait Post. 28 (1), 93–100.
Maharaj, J.N., Cresswell, A.G., Lichtwark, G.A., 2016. The mechanical function of the tibialis posterior muscle and its tendon during locomotion. J. Biomech. 49 (14), 3238–3243.

Maharaj, J.N., Cresswell, A.G., Lichtwark, G.A., 2017. Subtalar joint pronation and energy absorption requirements during walking are related to tibialis posterior tendinous tissue strain. Sci. Rep. 7 (1), 17958.
Mann, R.A., 1975. Biomechanics of the foot. In: American Academy of Orthopaedic Surgeons. Atlas of Orthotics, Biomechanical principles and application, pp. 257–266.
Manter, J.T., 1941. Movements of the subtalar and transverse tarsal joints. Anat. Rec. 80 (4), 397–410.
Nester, C.J., Findlow, A., Bowker, P., 2001. Scientific approach to the axis of rotation at the midtarsal joint. J. Am. Podiatr. Med. Assoc. 91 (2), 68–73.
Nester, C., Bowker, P., Bowden, P., 2002. Kinematics of the midtarsal joint during standing leg rotation. J. Am. Podiatr. Med. Assoc. 92 (2), 77–81.
Nester, C., Jones, R.K., Liu, A., Howard, D., Lundberg, A., Arndt, A., Lundgren, P., Stacoff, A., Wolf, P., 2007. Foot kinematics during walking measured using bone and surface mounted markers. J. Biomech. 40 (15), 3412–3423.
Niki, H., Ching, R.P., Kiser, P., Sangeorzan, B.J., 2001. The effect of posterior tibial tendon dysfunction on hindfoot kinematics. Foot Ankle Int. 22 (4), 292–300.
Okita, N., Meyers, S.A., Challis, J.H., Sharkey, N.A., 2014. Midtarsal joint locking: new perspectives on an old paradigm. J. Orthop. Res. 32 (1), 110–115.
Phan, C.B., Koo, S., 2015. Predicting anatomical landmarks and bone morphology of the femur using local region matching. Int. J. Comput. Assist. Radiol. Surg. 10, 1711–1719.
Phan, C.B., Nguyen, D.P., Lee, K.M., Koo, S., 2018. Relative movement on the articular surfaces of the tibiotalar and subtalar joints during walking. Bone Joint Res. 7 (8), 501–507.
Rodríguez, P.G., Polo, M.E., Cuartero, A., Felicísimo, Á.M., Ruiz-Cuetos, J.C., 2014. VecStatGraphs2D, a tool for the analysis of two-dimensional vector data: an example using QuikSCAT ocean winds. Geosci. Remote Sens. Lett. 11 (5), 921–925.
Tweed, J.L., Campbell, J.A., Thompson, R.J., Curran, M.J., 2008. The function of the midtarsal joint: a review of the literature. Foot 18 (2), 106–112.
Wang, B., Roach, K.E., Kapron, A.L., Fiorentino, N.M., Saltzman, C.L., Singer, M., Anderson, A.E., 2015. Accuracy and feasibility of high-speed dual fluoroscopy and model-based tracking to measure in vivo ankle arthrokinematics. Gait Post. 41 (4), 888–893.
Wang, M.C., Geng, X., Wang, S., Ma, M.X., Wang, M.X., Huang, M.J., Zhang, M.C., Chen, M.L., Yang, J., Wang, K., 2016. In vivo kinematic study of the tarsal joints complex based on fluoroscopic 3D–2D registration technique. Gait Post. 49, 54–60.
Wu, G., Siegler, S., Allard, P., Kirtley, C., Leardini, A., Rosenbaum, D., Whittle, M., D'Lima, D., Cristofolini, L., Witte, H., Schmid, O., 2002. ISB recommendation on definitions of joint coordinate system of various joints for the reporting of human joint motion—part I: ankle, hip, and spine. J. Biomech. 35 (4), 543–548.